Journal of Metals, Materials and Minerals, 34(1), 1777, 2024

Hot corrosion behavior of Mg_2SiO_4 ceramic exposed to molten Na_2SO_4 at 900°C to 1100°C

Hamza MILLES[1,*], Louafi SNANI[1], Amel OULABBAS[2], and Khaled TOUALBIA[3]

[1] *Department of Metallurgy and Materials Engineering, Badji Mokhtar-Annaba University, P.O Box.12, Annaba, 23000, Algeria*
[2] *Research Centre in Industrial Technologies (CRTI) P.O.Box 64, Cheraga, 16014 Algiers, Algeria*
[3] *Department of Material Sciences, Abbes Laghrour University, Road of Batna, Khenchela, 40004, Algeria*

***Corresponding author e-mail**: m.hamza05@yahoo.fr

Received date:
2 July 2023
Revised date
17 January 2024
Accepted date:
6 March 2024

Keywords:
Forsterite;
Thermal barrier;
Hot corrosion;
Molten salt

Abstract

Thermal barriers are used as protective coating for critical components working at high temperature of gas turbines. Forsterite (Mg_2SiO_4) ceramic is proposed by researchers as a novel thermal barrier coating (TBC), due to its low thermal conductivity and good thermal expansion. Hot corrosion results from the molten salts effect on the TBC's surface, accumulated during the combustion processes. In this study, Mg_2SiO_4 samples were exposed to Na_2SO_4 molten salt at 900°C, 1000°C and 1100°C for 6 h in air. Samples were investigated and compared using scanning electron microscope (SEM) and X-Ray diffractometer (XRD). $MgSO_4$ was the predominant corrosion product observed on the surface of the samples. $Na_2Mg_5Si_{12}O_{30}$ was also observed at 1000°C and 1100°C, and Na_2SiO_3 appeared only on sample treated at 900°C.

1. Introduction

Forsterite is a crystalline magnesium silicate belongs to the olivine group with chemical formula Mg_2SiO_4. It was systematically investigated for thermal barrier coating (TBC) applications. Mg_2SiO_4 produced via solid-state reaction has high phase stability up to 1300°C, according to the results. At 1000°C, the thermal conductivity of Mg_2SiO_4 was 20% lower than that of yttria stabilized zirconia (8YSZ). Mg_2SiO_4 also presented moderate thermal expansion coefficients, which increased from 8.6×10^{-6} °C^{-1} to 11.3×10^{-6} °C^{-1} (200°C to 1350°C) [1]. Forsterite is an important material in the magnesia–silica system [2]. This ceramic demonstrated a considerable increase in fracture toughness over hydroxyapatite ceramics (KIC = 2.4 MPa·m$^{-1/2}$), exceeding the minimum limit stated for bone implant. In vitro studies showed significant osteoblast adhesion, spreading, and growth on the surface of forsterite ceramic [3]. Ni *et al*. [3,4] showed that forsterite is a new bioceramic with excellent mechanical characteristics and good biocompatibility that may be ideal for hard tissue repair. On the hot section components of gas turbines, thermal barrier coatings (TBCs) have been thickly applied in order to shield them from heat, corrosion, and erosion [5,6]. Due to its inherent physical characteristics and compatibility with superalloys, yttria-stabilized zirconia (YSZ), which has a 6 wt% to 8 wt% composition, is currently the most successful TBC material [7,8]. However, due to the hazardous phase transitions of YSZ at this temperature, which are accompanied by a significant volume change of 4% to 6% [9], the long-term application temperature of YSZ is restricted to below 1200°C. TBCs are used more frequently in industrial engines used on land as well as marine engines, they frequently work in extreme conditions or burn fuels of poor quality that contain contaminants like vanadium, sulfur, and sodium. During turbine engine operation, these contaminants can condense on the surface of TBCs at temperatures ranging from 600°C to 1100°C [10,11]. Na_2SO_4 and $NaVO_3$ are the two primary salts found in the molten salt deposits. High-temperature materials used in combustion systems are severely corroded by molten sulfate-vanadate deposits that form as a result of the condensation of these fuels' combustion products [12]. To improve their applications, it is necessary to investigate the hot corrosion behavior of TBCs in the presence of contaminants found in low-quality fuels. Previous studies have shown that YSZ is susceptible to corrosive attack by molten salts [13,14]. Molten salts could leach away the stabilizer yttria in YSZ during a long-term operation at high temperatures, resulting in the instability of the tetragonal phase and transformation to the monoclinic phase upon cooling [15,16]. There seems to be an urgent need to investigate alternate TBC materials in order to increase hot corrosion resistance and phase stability [17,18]. As interesting TBC, prospects for higher temperature applications materials including pyrochlore-type $Ln_2Zr_2O_7$ (Ln = La to Gd) [19], perovskite-type $SrZrO_3$ [20], fluorite-type $La_2Ce_2O_7$ [13], and magnetoplumbite-type $LnMgAl_{11}O_{19}$ (Ln = La, Nd, Sm, Gd) [21,22] have also been put forth. Among these, Mg_2SiO_4 has been demonstrated to have some great properties for the use of TBC, and has been evaluated as a potential TBC material at high temperatures Vanadium in low-quality fuels reacts with oxygen to form a highly corrosive acidic oxide V_2O_5, this might result in hot corrosion of TBCs during high-temperature combustion [1]. To examine Mg_2SiO_4's suitability as a new TBC material, It is initially required to comprehend its hot corrosion performance in a corrosive environment. The microstructures and characteristics of Mg_2SiO_4 subjected to molten Na_2SO_4 deposits are, nevertheless, little understood. Sodium sulfate has been confirmed as the main chemical reagent involved in hot corrosion, due to its exceptional stability over a wide range of temperatures and oxygen partial pressures [23-25]. The generation of Na_2SO_4 is mainly the result of oxidation or combustion of impurities containing sulfur and alkali metals in fuels and aerosols present in the air. This work aims to assess the hot corrosion behavior of Mg_2SiO_4 ceramic exposed to molten Na_2SO_4 at various temperatures where TBCs fail more rapidly in hot corrosion.

2. Experimental

In this study, forsterite was obtained using pure magnesium carbonate $4MgCO_3Mg\ (OH)_{24}H_2O$ (S.G.I.M. S.p.A) and talc $Mg_3Si_4O_{10}(OH)_2$ (BIOCARE Laboratories) as starting materials. Figure 1 illustrates the experimental procedure flow chart. Magnesium carbonate was annealed at 1000°C for 1 h to obtain MgO. A mixture of MgO and talc at a molar ratio of 5:1 was ball-milled in a planetary ball-mill (FRITSH PULVERISETTE7) under ambient conditions, using six 10 mm stainless steel balls in a stainless-steel jar (80 mL). The ball-to-powder weight was approximately 10:1, and the rotation speed of the main disc was set at 500 rpm during 5 h, and then, an annealing was carried at 1000°C for 1h in the air [26]. The Forsterite powder was uniaxially compacted in a θ 20 mm die by ambient isostatic pressing at 4500 KPa, and then, the obtained green bodies were calcinated at 1600°C for 3 h. Obtained pellets were carried out for hot corrosion test in presence of molten sodium sulfate Na_2SO_4 in a muffle furnace. Na_2SO_4 powder was spread out uniformly on the specimen's surface with a concentration of 20 mg·cm^{-2}. Thereafter, samples were subjected to isotherm heat treatment at 900°C, 1000°C and 1100°C for 6 h in an ambient atmosphere, and cooled down to the room temperature in the furnace. Following a cyclic high-temperature corrosion test (four cycles of one hour and one cycle of twelve hours), the mass change values of each sample were measured to determine the kinetics of hot corrosion. The weight change was measured using an electronic balance with a sensitivity of 0.01 mg.

In order to specify the corrosion attack, the phase analysis of Mg_2SiO_4 ceramic were performed after hot corrosion tests, samples were characterized by X-ray diffraction (XRD) and scanning electron microscopy (SEM). XRD patterns were obtained using Rigaku Ultima IV X-Ray diffractometer using Cu Kα radiation, recorded in the 2θ range of 10° to 100° (step size 0.01° and time per step 1 s), and compared to the Joint Committee on Powder Diffraction and Standards (JCDPS). The Reference Intensity Ratio (RIR) was used for quantitative analysis. The material degradation was characterized by observing the samples surfaces and cross sections using scanning electron microscopy (SEM FEI Quanta 250)

3. Results

The morphological shape of the obtained forsterite powder is shown in Figure 2(a). Particles have an irregular flat shape resulting from the ball-milling process. Several micrographs were used to measure particles size, and it was between 3 µm and 35 µm. Figure 3 illustrates XRD pattern of the synthesized powder, which matches well with forsterite standard JCDP card (No.78-1371). Enstatite ($MgSiO_3$) is also present with the forsterite phase. The crystallite size of the forsterite is in the range of 33 nm to 166 nm and that one of the enstatite is in the range of 34 nm to 177 nm. Figure 4 shows the sample surface as received and after reaction at different temperatures for 6 h. Visual inspection of the sample surfaces after exposure revealed changes in colour and surface morphology. Opaque droplets were formed, indicating that corrosive reactions had occurred, and a transparent reacting layer formed over the entire surface of the specimens. After the hot corrosion test, XRD diagrams of the corroded surface in Figure 5 show distinct peaks from magnesium sulphate ($MgSO_4$, JCPDS No. 74-1364) and enstatite ($MgSiO_3$, JCPDS No. 72-0439).

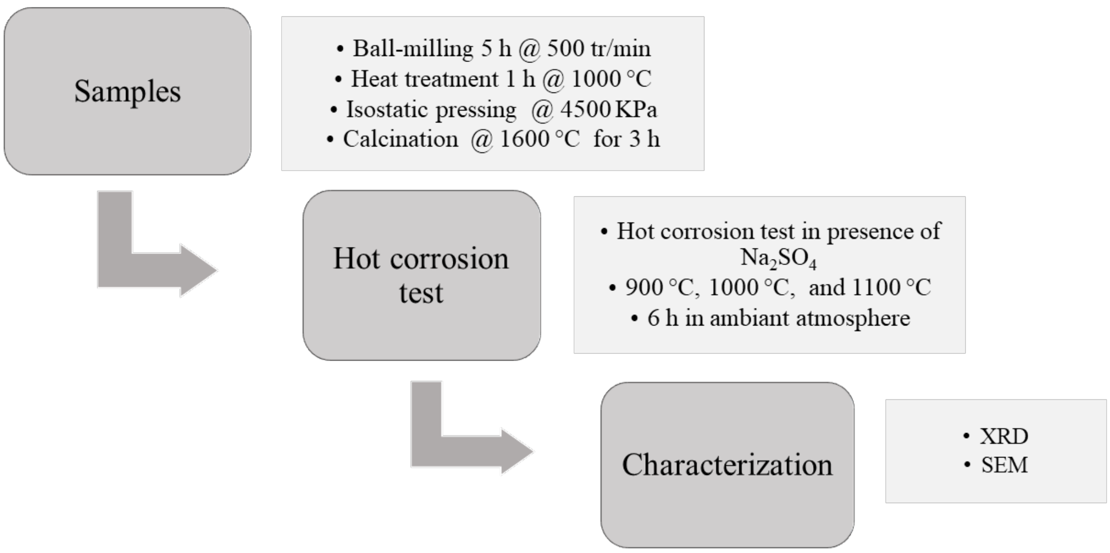

Figure 1. Experimental procedure flow chart.

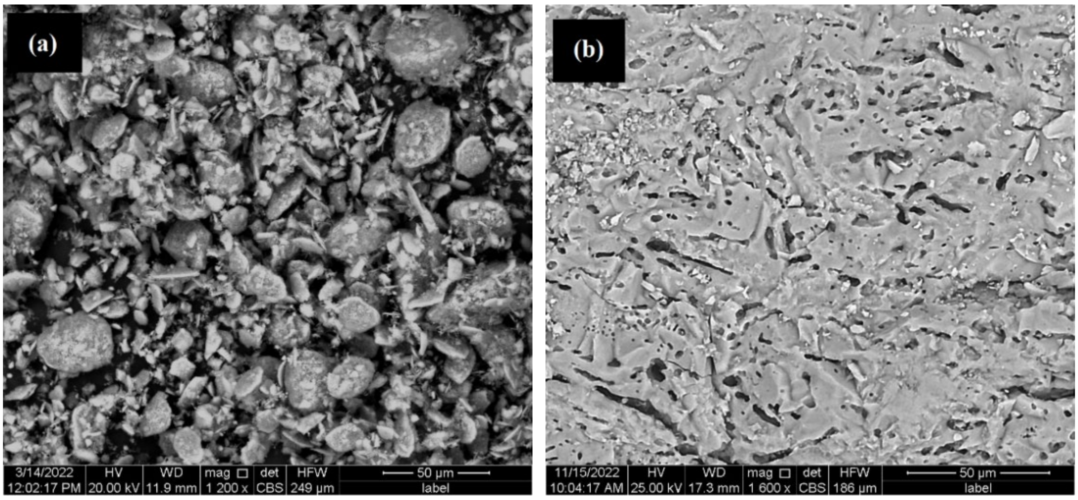

Figure 2. SEM micrograph of: (a) Obtained forsterite powder, and (b) Cross section of the sample before hot corrosion test.

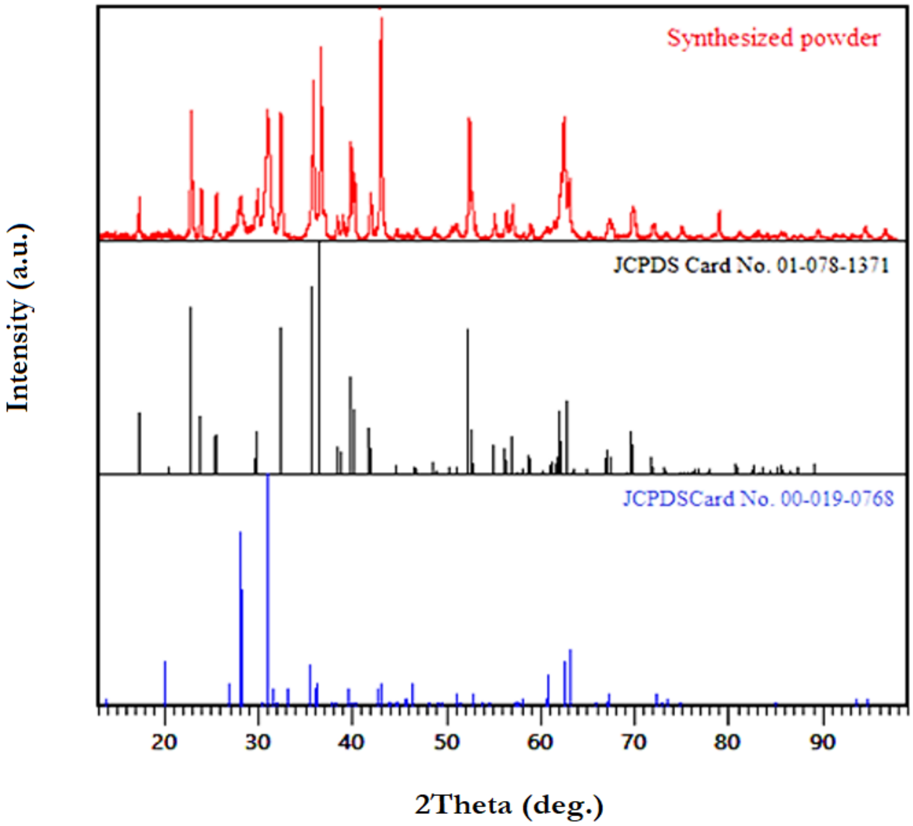

Figure 3. XRD patterns of synthesized forsterite powder.

Tables 1. Phase composition of surface after hot corrosion.

Temperature (°C)	Phase composition of surface after hot corrosion (wt%)
900	73 Mg_2SiO_4 + 5 $MgSO_4$ + 14 $MgSiO_3$ + 8 Na_2SiO_3
1000	79 Mg_2SiO_4 + 2 $MgSO_4$ + 11 $MgSiO_3$ + 8 $Na_2Mg_5Si_{12}O_{30}$
1100	71 Mg_2SiO_4 + 3 $MgSO_4$ +14 $MgSiO_3$ + 12 $Na_2Mg_5Si_{12}O_{30}$

The absence of any remaining Na_2SO_4 characteristic peaks suggests that the whole amount was consumed during hot corrosion. Sodium silicate (Na_2SiO_3, JCPDS No. 73-2115), another phase produced by hot corrosion, was also seen. Therefore, based on their peak intensities, the mole fractions of $MgSO_4$ and Na_2SiO_3 were roughly obtained, and the findings are shown in Table 1. Notably, the main phase in the temperature range of the test is invariably Mg_2SiO_4

The surface morphology of Na_2SO_4 coating on Mg_2SiO_4 samples subjected to heat treatment at 900°C, 1000°C, and 1100°C for a duration of 6 h is presented in Figure 4, respectively. The spontaneous arrangement of corrosion products engenders a novel superimposition on the Mg_2SiO_4 ceramic surface. Figure 6(a) and Figure 6(b) depicting the surface morphology of the specimens corroded at temperatures of 900°C and 1000°C. The analytical findings obtained from the energy-dispersive X-ray spectroscopy (EDS) are presented in Figure 6(g). The analysis revealed that the resultant corrosion product was a blend of magnesium (Mg), silicon (Si), sodium (Na), sulfur (S), and oxygen (O).

In conjunction with the aforementioned XRD and EDS findings, additional analyses indicate that the chemical composition of the compound was comprised of magnesium silicate (Mg_2SiO_4), magnesium sulfate ($MgSO_4$), and sodium silicate (Na_2SiO_3). When the temperature increased to 1000°C, the extent of the attack was found to be highly localised. Furthermore, the reaction products were randomly distributed on the sample's surface (Figure 6(b) and Figure 6(e)).

According to EDS results, the corrosion product has been determined was mainly composed of Mg, Si, O, and Na. The XRD pattern illustrated in Figure 5(b) validates that the corrosion products are as described in Table 1. Upon elevating the temperature to 1100°C, identical reaction products were observed as delineated in Figure 6(c) and Figure 6(f). It has been observed that the aforementioned compounds occur in lesser quantities. The formation of tiny idiomorphic crystals on the surface of the corroded sample at 1100°C could be identified as forsterite.

When the annealing temperature rises from 900°C to 1000°C, the content of $MgSO_4$ phase decreased, with appearance of a new compound ($Na_2Mg_5Si_{12}O_{30}$, JCPDS No. 73-0929). After corroded at 1100°C, in Figure 5 Pattern (c), the sharp peaks ascribed to Mg_2SiO_4 accounted for 71% of the total crystalline phase of the surface, while the relative content of the sodium magnesium silicate further increased from 8% at 1000°C to 12% at 1100°C. Cross-sectional SEM micro-graphs of the hot-corroded samples in Figure 7 were examined. After degradation by Na_2SO_4 at 900°C for 6 h, in Figure 7(a), the Mg_2SiO_4 ceramic degraded only slightly, as the microstructure isn't significantly different from the uncorroded Mg_2SiO_4 ceramic shown in Figure 2(b). As the corrosion temperature increased to 1000°C (Figure 7(b)) some localised pits were formed. These pits are attributed to localised attack at structural discontinuities such as grain boundaries, pores or cracks. Thus, exposure of Mg_2SiO_4 to Na_2SO_4 creates temperature-dependent attack morphologies based on the melting temperature of the reaction layer. At 1100°C, traces of corrosion products appear deep in the sample as shown in Figure 7(c). This indicates that the high porosity of the Mg_2SiO_4 ceramic is the primary reason of the infiltration's frequent occurrence.

When compared to samples treated at lower temperatures, those treated at 1100°C gained more weight. Figure 8 depicts the corrosion rate and kinetic behaviour. The reaction kinetics of the samples follows a parabolic growth rate. The parabolic rate constant, Kp, is calculated using the following equation:

$$\left(\frac{\Delta W}{A}\right)^2 = Kp\ t \tag{1}$$

Where:

$\left(\frac{\Delta W}{A}\right)^2$ = Weight gain per unit area ($mg \cdot cm^{-2}$),

Kp = Parabolic rate constant ($mg \cdot cm^{-4} \cdot s^{-1}$),

T = Time (s).

Results found are 1.792×10^{-3} $mg \cdot cm^{-4} \cdot s^{-1}$, 2.503×10^{-3} $mg \cdot cm^{-4} \cdot s^{-1}$, and 2.903×10^{-3} $mg \cdot cm^{-4} \cdot s^{-1}$, respectively for the samples treated at 900°C, 1000°C, and 1100°C.

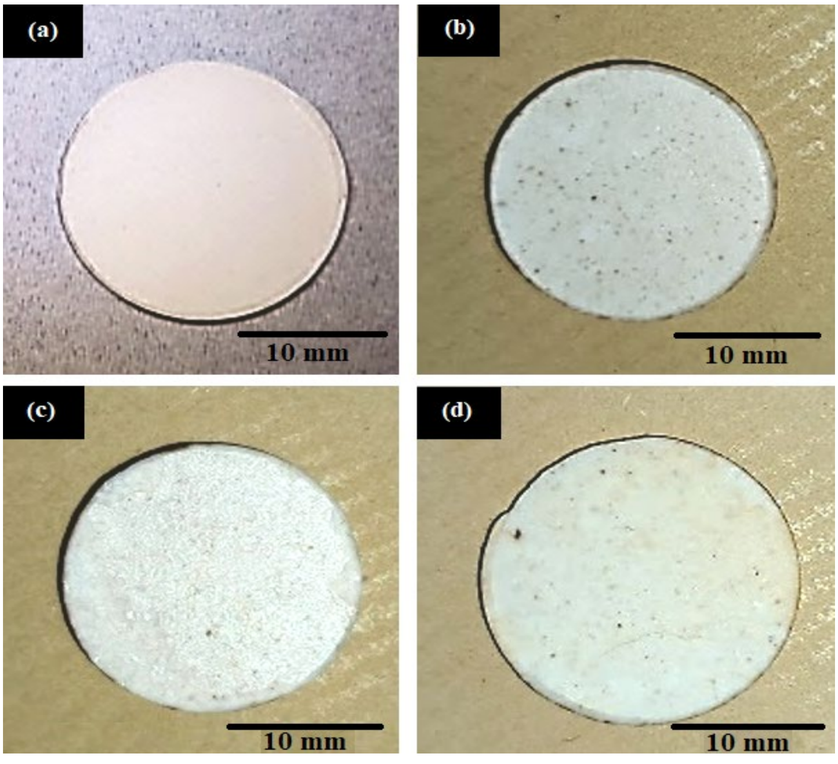

Figure 4. Surface of samples before and after hot corrosion tests for 6 h. (a) before, (b) at 900°C; (c) at 1000°C, and (d) at 1100°C.

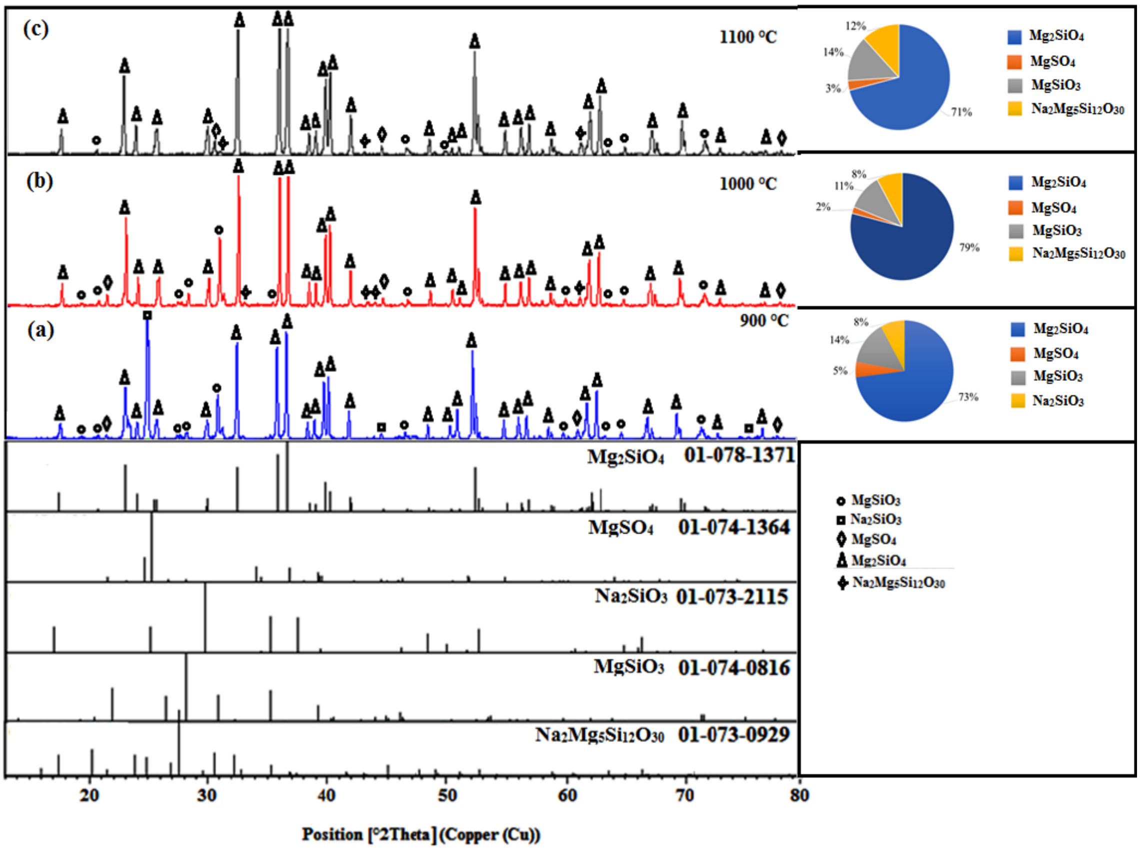

Figure 5. XRD patterns of samples treated at (a) 900°C, (b) 1000°C, and (c) 1100°C.

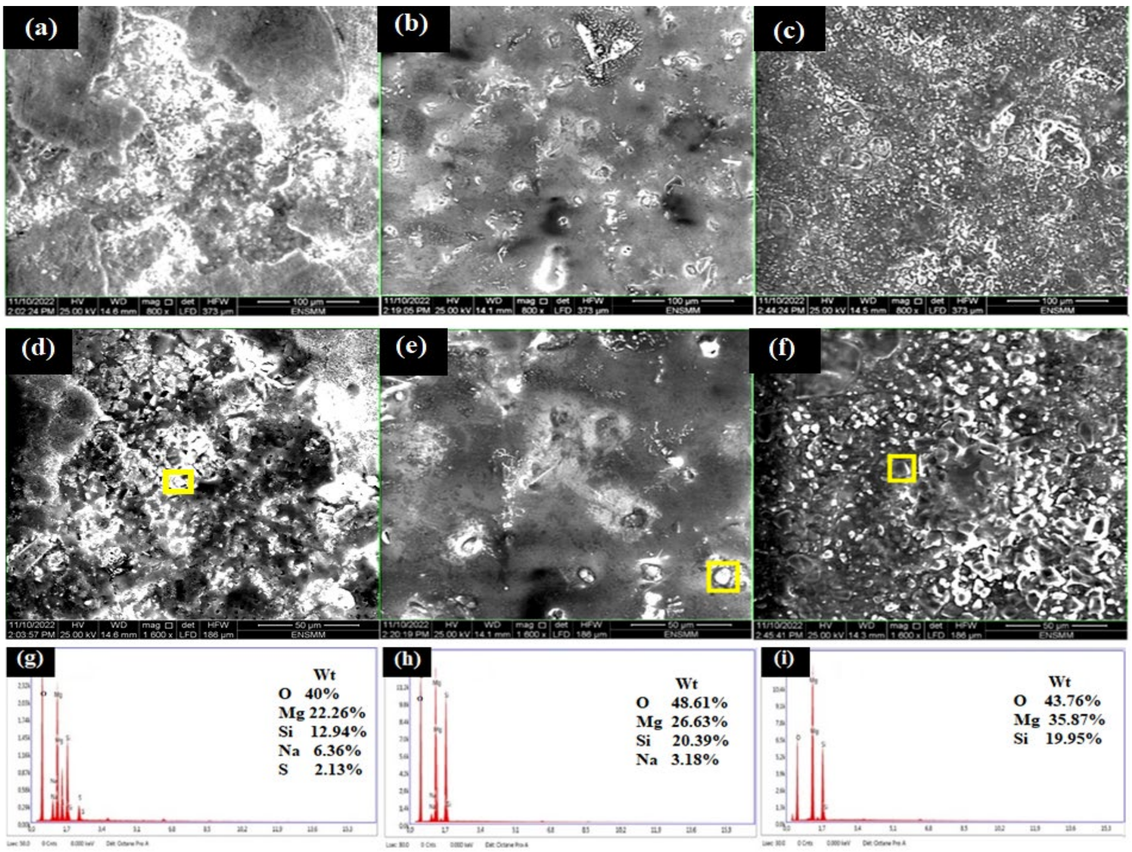

Figure 6. Forsterite microstructure after hot corrosion tests in presence of Na_2SO_4. (a), (b), and (c) Low magnification micrographs of samples heat-treated at 900°C, 1000°C, and 1100°C; (d), (e) and (f) high-magnification of (a), (b) and (c) respectively; (g), (h) and (i) indicate the compound chemical analysis.

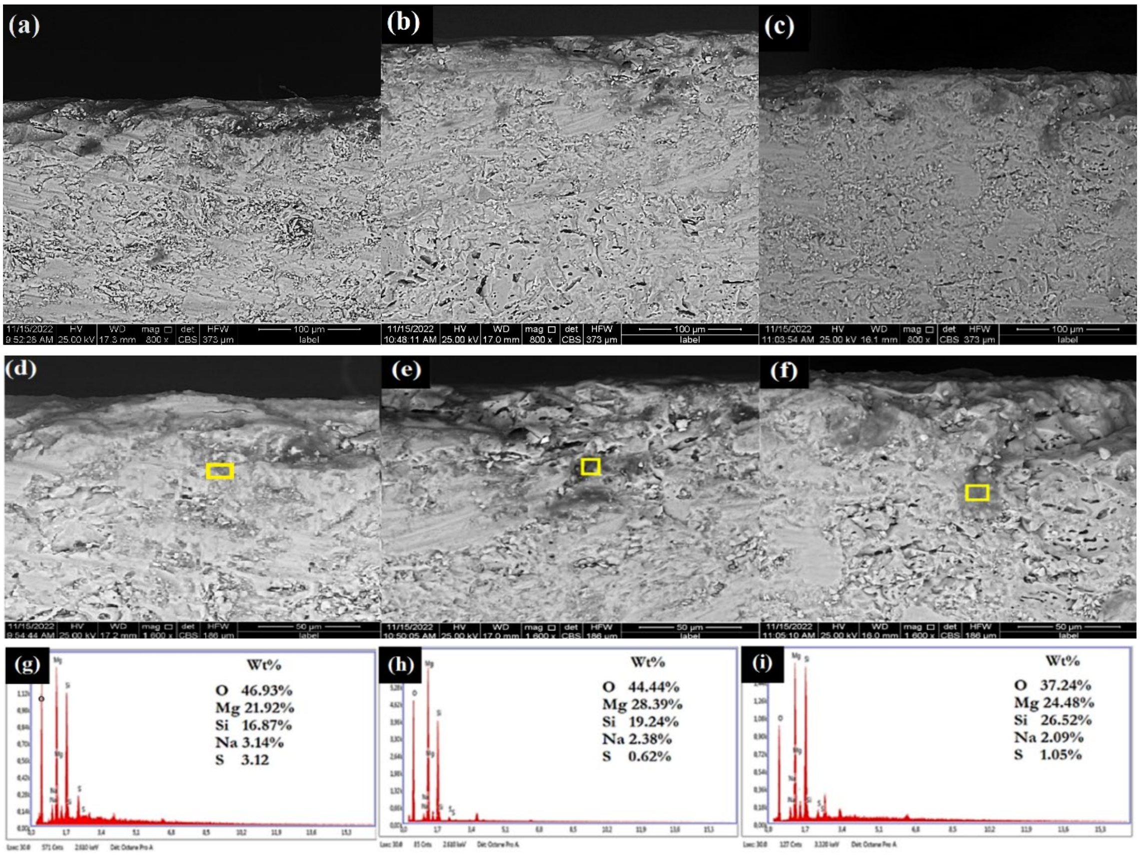

Figure 7. Cross-sectional SEM micrographs of samples after hot corrosion tests at 900°C, 1000°C, and 1100°C respectively; (a), (b) and (c) Low magnification micrographs, (d), (e) and (f) High magnification micrographs; (g), (h) and (i) indicate the compound chemical analysis.

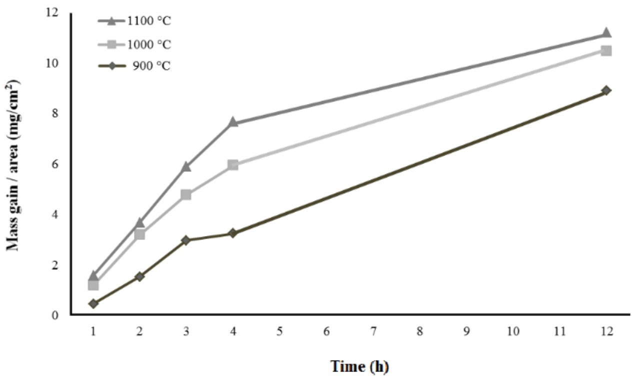

Figure 8. Mass gain vs. time for samples treated at 900°C, 1000°C, and 1100°C.

4. Discussion

High-temperature corrosion phenomena of forsterite were studied in the presence of molten Na_2SO_4 salt in the temperature range from 900°C to 1100°C in air. Results revealed that the principal corrosion product is $MgSO_4$, which melts at 1185°C (greater than the corrosion temperature) [27]. The ceramics were attacked by Na_2SO_4 according to the following Equations:

At 900°C:

$$Na_2SO_4\ (liq) \rightarrow Na_2O\ (liq) + SO_3\ (g) \quad (2)$$

$$Mg_2SiO_4\ (s) + SO_3\ (g) \rightarrow MgSO_4\ (s) + MgSiO_3\ (s) \quad (3)$$

$$MgSiO_3 + Na_2O + SO_3 \rightarrow Na_2SiO_3 + MgSO_4 \quad (4)$$

At 1000°C and more:

$$5MgSiO_3 + Na_2SiO_3 + 6SiO_2 \rightarrow Na_2Mg_5Si_{12}O_{30} \quad (5)$$

The molten salt attack breaks the existing chemical bonds, followed by the formation of a new compound with new chemical bonds, which is the more fundamental process behind the molten salt chemical reaction [28]. Hou Y *et al*. [29] provided an overview of the Mg_2SiO_4 bond categorization. Figure 9 depicts the several chemical bonds that make up Mg_2SiO_4. Chemical bonds between Si and O have greater bond energies than those between Mg and O, according to Table 2's listing of bond energies. As a result, Si-O bonds in Mg_2SiO_4 crystal are more resistant to being destroyed by the attack of the molten salts [30]. Based on phase diagrams and thermodynamics, the formation of $MgSO_4$ and $MgSiO_3$ can be consistently detected at all corrosion temperature levels from 900°C to 1100°C. It is generally accepted that hot corrosion at elevated temperatures should obey the Lewis acid-base rule [28,31].

The presence of new compounds indicates a reaction between Na_2SO_4 and the sample material. At 900°C, the corrosion product detected by XRD pattern in Figure 04 is Na_2SiO_3, this compound disappeared at 1000°C and formed a new complex $Na_2Mg_5Si_{12}O_{30}$ indicating an oxidation increased with increasing temperature, $MgSO_4$ was also detected in all samples. The corrosion attack is slightly observed on the surface of the samples in Figure 06, by apparition of some localized pits. And in depth, the attack was observed by the presence of the corrosion products due to infiltration of the molten salt through pores and grain boundaries or discontinuities, with absence of any significant film growth after hot corrosion tests (Figure 07).

However, it was found that the amount of $MgSO_4$ on the damaged surface was simultaneously decreasing when the corrosion temperature increased to 1000°C. Moreover, the corrosion product $Na_2Mg_5Si_{12}O_{30}$ was mainly present on the surface at 1000°C and 1100°C (Table 1), both on the surface and pores of the cross-section, while the $MgSiO_3$ was detected on the surface.

Forsterite behaviors in the same way as YSZ against the hot corrosion in presence of Na_2SO_4, so, it follows parabolic rate kinetics, which indicates that the corrosion is governed by diffusion growth, with a higher mass gain of forsterite at 900°C. The higher weight gain and corrosion rate are observed, at 1100°C, and the parabolic growth rate indicates that the oxidation process diffusion controlled and governed by outer cation and inner anion migration [33].

P. Vadasz *et al*. [34] studied the MgO–SiO_2–Na_2O system in the isothermal part of the ternary diagram at 1300°C (Figure 10) and found that Mg_2SiO_4 is stable when mixed with Na_2O. This is supported by the XRD results, all of which show strong diffraction peaks from his Mg_2SiO_4 on the corroded surface of the samples under various corrosion conditions. Since excess molten Na_2SO_4 was used in our study, the presence of the Mg_2SiO_4 phase may indicate a very stable phase with less tendency to react with Na_2SO_4 in the melt. Combined with the above analysis, the degradation process of Mg_2SiO_4 ceramics in the presence of molten Na_2SO_4 is deduced as follows. When Mg_2SiO_4 coexists with Na_2SO_4 at any corrosion temperature level from 900°C to 1100°C, a liquid phase containing Na, Mg, Si and O is formed, after saturation a new phase such as $Na_2Mg_5Si_{12}O_{30}$ precipitates. The higher corrosion rate above 1000°C is caused by the melting of the salt and the development of basic and acidic fluxes on the surfaces of the samples [35]. It can be reasonably assumed that the degradation of Mg_2SiO_4 by Na_2SO_4 is mainly caused by thermo-mechanical damage rather than by thermochemical attack. Therefore, the approach of introducing chemically inert oxides to improve hot corrosion resistance appears to be less effective than expected.

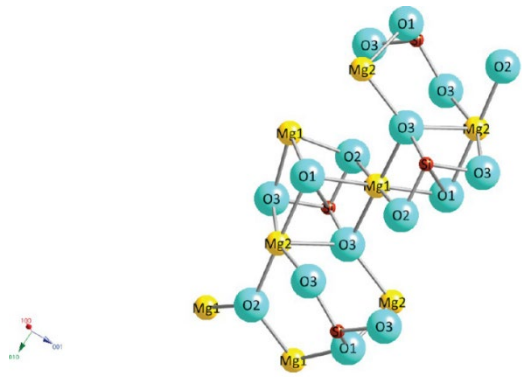

Figure 9. Crystal structure of forsterite [32].

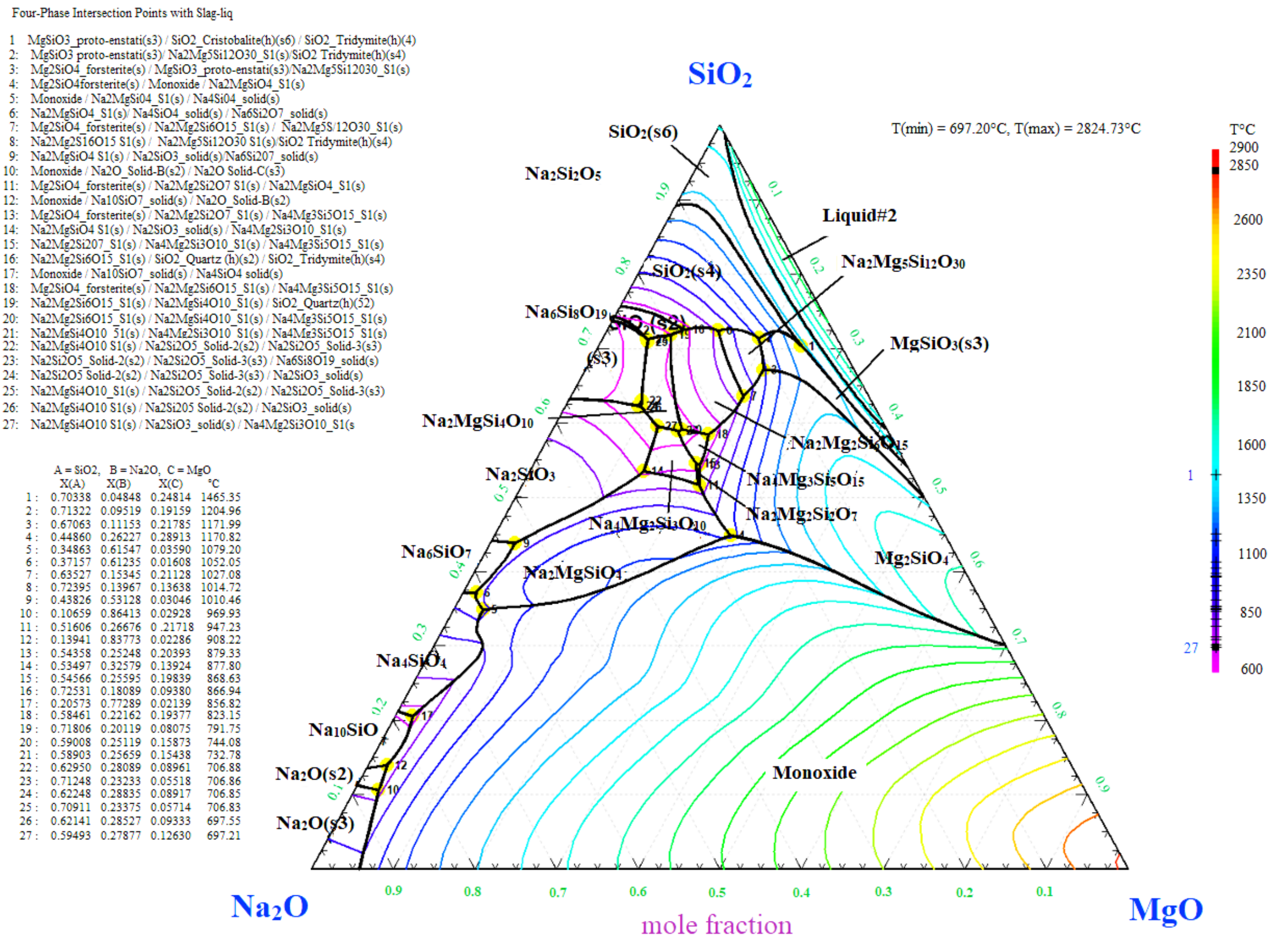

Figure 10. Ternary diagram of the SiO_2–Na_2O–MgO system [36].

Table 2. Bond classification of Mg_2SiO_4 [29].

Bond type	d (Å)	E ($e^2\cdot Å^{-1}$)
Mg1-O1	2.085	1.918
Mg1-O2	2.069	1.933
Mg1-O3	2.123	1.876
Mg2-O1	2.183	1.832
Mg2-O2	2.051	1.950
Mg2-O3	2.067	1.805
Mg2-O3*	2.216	1.953
Si-O1	1.615	4.954
Si-O2	1.634	4.837
Si-O3	1.635	4.893

5. Conclusions

In this study, we investigated the behavior of forsterite in contact with Na_2SO_4 at high temperatures. The main points drawn are:

1) Forsterite is not immune to alterations caused by molten salts, which is reflected by the formation of products resulting from chemical reactions with Na_2SO_4

2) According to the XRD curves, the main compound detected is magnesium sulfate ($MgSO_4$) accompanied by $MgSiO_3$, the latter has a lower melting point than forsterite and these two phases coexist in all the results,

3) At 900°C, in addition to the previous phases, we detected sodium silicates Na_2SiO_3,

4) At 1000°C and 1100°C, a new compound $Na_2Mg_5Si_{12}O_{30}$ appeared with the disappearance of Na_2SiO_3,

5) The surface of the samples was slightly altered at 900°C and 1000°C under the effect of the salt, with no degradation in-depth, however, at 1100°C, the attack is accentuated on the surface and goes in-depth by following the defects such as the pores and the cracks.

The best corrosion protection is found in TBCs with advanced ceramics and optimized coatings, according to studies on the hot corrosion behavior of different TBC varieties. Consequently, it is crucial that research endeavors persist in order to enhance our comprehension of the degradation mechanisms and create effective approaches to prevent the degradation of TBCs caused by hot corrosion. Forsterite was studied for thermal barrier coating applications in which TBC is subjected to corrosion at high temperatures in the presence of molten salts such as Na_2SiO_4 and V_2O_5. It has shown promising results in thermal cycling and hot corrosion tests [30]. The results revealed that Mg_2SiO_4 has good phase stability up to 1300°C, and its thermal conductivity at 1000°C is 20% lower than that of 8YSZ, with moderate thermal expansion. [01] Hence, forsterite has the potential to serve as a new TBC material.

References

[1] S. Chen, X. Zhou, W. Song, J. Sun, H. Zhang, J. Jiang, L. Deng, S. Dong, and X. Cao, "Mg_2SiO_4 as a novel thermal barrier coating material for gas turbine applications," *Journal of the European Ceramic Society,* vol. 39, pp. 2397-2408, 2019.

[2] M. H. Fathi and M. Kharaziha, "Mechanically activated crystallization of phase pure nanocrystalline forsterite powders," *Materials Letters*, vol. 62, no. 27, pp. 4306-4309, 2008.

[3] S. Ni, L. Chou, and J. Chang, "Preparation and characterization of forsterite (Mg_2SiO_4) bioceramics," *Ceramics International*, vol. 33, no. 1, pp. 83-88, 2007.

[4] S. Ni, J. Chang, and L. Chou, "In vitro studies of novel CaO–SiO_2–MgO system composite bioceramics," *Journal of Materials Science: Materials in Medicine*, vol. 19, no. 1, pp. 359-367, 2007.

[5] N. P. Padture, M. Gell, and E. H. Jordan, "Thermal barrier coatings for gas-turbine engine applications," *Science*, vol. 296, no. 5566, pp. 280-284, 2002.

[6] R. Vaßen, F. Cernuschi, G. Rizzi, A. Scrivani, N. Markocsan, L. Östergren, A. Kloosterman, R. Mevrel, J. Feist, and J. Nicholls, "Recent activities in the field of thermal barrier coatings including burner rig testing in the European Union," *Advanced Engineering Materials*, vol. 10, no. 10, pp. 907-921, 2008.

[7] J. T. DeMasi-Marcin and D. K. Gupta, "Protective coatings in the gas turbine engine," *Surface and Coatings Technology*, vol. 68-69, pp. 1-9, 1994.

[8] R. Vassen, X. Cao, F. Tietz, D. Basu, and D. Stöver, "Zirconates as new materials for thermal barrier coatings," *Journal of the American Ceramic Society*, vol. 83, no. 8, pp. 2023-2028, 2004.

[9] Z.-G. Liu, J.-H. Ouyang, and Y. Zhou, "Influence of gadolinia on thermal expansion property of ZrO_2– 4.5 mol% Y_2O_3 ceramics," *Journal of Alloys and Compounds*, vol. 473, no. 1-2, 2009.

[10] X. H. Zhong, Y. M. Wang, Z. H. Xu, Y. F. Zhang, J. F. Zhang, and X. Q. Cao, "Hot-corrosion behaviors of overlay-clad yttria-stabilized zirconia coatings in contact with vanadate–sulfate salts," *Journal of the European Ceramic* Society, vol. 30, no. 6, pp. 1401-1408, 2010.

[11] N. Wu, Z. Chen, and S. X. Mao, "Hot corrosion mechanism of composite alumina/yttria-stabilized zirconia coating in molten sulfate-vanadate salt," *Journal of the American Ceramic Society*, vol. 88, no. 3, pp. 675-682, 2005.

[12] T. S. Sidhu, R. D. Agrawal, and S. Prakash, "Hot corrosion of some superalloys and role of high-velocity oxy-fuel spray coatings—a review," *Surface and Coatings Technology*, vol. 198, no. 1-3, pp. 441-446, 2005.

[13] H. Dong, D. Wang, Y. Pei, H. Li, P. Li, and W. Ma, "Optimization and thermal cycling behavior of $La_2Ce_2O_7$ thermal barrier coatings," *Ceramics International*, vol. 39, no. 2, pp. 1863-1870, 2013.

[14] S. Li, Z.-G. Liu, and J.-H. Ouyang, "Growth of $YbVO_4$ crystals evolved from hot corrosion reactions of $Yb_2Zr_2O_7$

against V_2O_5 and Na_2SO_4+V_2O_5," *Applied Surface Science*, vol. 276, pp. 653-659, 2013.

[15] B. R. Marple, J. Voyer, M. Thibodeau, D. R. Nagy, and R. Vassen, "Hot corrosion of lanthanum zirconate and partially stabilized zirconia thermal barrier coatings," *Journal of Engineering for Gas Turbines and Power*, vol. 128, no. 1, pp. 144-152, 2004.

[16] L. Guo, C. Zhang, M. Li, W. Sun, Z. Zhang, and F. Ye, "Hot corrosion evaluation of Gd_2O_3-Yb_2O_3 co-doped Y_2O_3 stabilized ZrO_2 thermal barrier oxides exposed to Na_2SO_4+V_2O_5 Molten Salt," *Ceramics International*, vol. 43, no. 2, pp. 2780-2785, 2017.

[17] X. Q. Cao, R. Vassen, and D. Stoever, "Ceramic materials for thermal barrier coatings," *Journal of the European Ceramic Society*, vol. 24, no. 1, pp. 1-10, 2004.

[18] C. G. Levi, "Emerging materials and processes for thermal barrier systems," *Current Opinion in Solid State and Materials Science*, vol. 8, no. 1, pp. 77-91, 2004.

[19] W. Ma, D. Mack, R. Vaßen, and D. Stöver, "Perovskite-type strontium zirconate as a new material for thermal barrier coatings," *Journal of the American Ceramic Society*, vol. 91, no. 8, pp. 2630-2635, 2008.

[20] C. Friedrich, R. Gadow, and T. Schirmer, "Lanthanum hexaaluminate – A new material for atmospheric plasma spraying of advanced thermal barrier coatings," *Journal of Thermal Spray Technology*, vol. 10, no. 4, pp. 592-598, 2001.

[21] G. Li, and G. Yang, "Understanding of degradation-resistant behavior of nanostructured thermal barrier coatings with bimodal structure," *Journal of Materials Science & Technology*, vol. 35, no. 3, pp. 231-238, 2019.

[22] R. Vassen, X. Cao, F. Tietz, D. Basu, and D. Stöver, "Zirconates as new materials for thermal barrier coatings," *Journal of the American Ceramic Society*, vol. 83, no. 8, pp. 2023-2028, 2004.

[23] R. A. Rapp, and Y.-S. Zhang, "Hot corrosion of materials: fundamental studies," *JOM*, vol. 46, no. 12, pp. 47-55, 1994

[24] C. O. Park, and R. A. Rapp, "Electrochemical reactions in molten Na_2SO_4 at 900°C," *Journal of The Electrochemical Society*, vol. 133, no. 8, pp. 1636-1641, 1986.

[25] R. A. Rapp, "Chemistry and electrochemistry of hot corrosion of metals," *Materials Science and Engineering*, vol. 87, pp. 319-327, 1987

[26] F. Tavangarian, and R. Emadi, "Synthesis of nanocrystalline forsterite (Mg_2SiO_4) powder by combined mechanical activation and thermal treatment," *Materials Research Bulletin*, vol. 45, no. 4, pp. 388-391, 2010.

[27] J. Takahashi, Y. Kawai, and S. Shimada, "Hot corrosion of cordierite ceramics by Na^- and K^- salts," *Journal of the European Ceramic Society*, vol. 18, no. 8, pp. 1121-1129, 1998.

[28] X. Chen, X. Cao, B. Zou, J. Gong, and C. Sun, "Corrosion of lanthanum magnesium hexaaluminate as plasma-sprayed coating and as bulk material when exposed to molten V_2O_5-containing salt," *Corrosion Science*, vol. 91, pp. 185-194, 2015.

[29] Y. Hou, H. Zhu, S. Yan, S. Wang, and B. Hu, "Growth of Cr_4^+: Mg_2SiO_4 crystal by Czochralski method," *SPIE Proceedings*, vol. 1863, pp. 84-89, 1993.

[30] S. Chen, W. Song, X. Zhou, H. Zhang, X. Zhou, Y. Tu, J. Yuan, S. Dong, and X. Cao, "Hot corrosion of Mg_2SiO_4 ceramics exposed to V_2O_5 at temperatures of 700°C to 1050°C in air," *Corrosion Science*, vol. 159, p. 108114, 2019.

[31] S. Li, Z.-G. Liu, and J.-H. Ouyang, "Hot corrosion of (Sm1−xYbx) $2Zr_2O_7$ (x=0, 0.5, 1.0) ceramics against V_2O_5 molten salt in air at 800°C," *International Journal of Applied Ceramic Technology*, vol. 9, no. 1, pp. 149-158, 2011.

[32] V. Prigiobbe, A. S. Negreira, and J. Wilcox, "Interaction between olivine and water based on density functional theory calculations," *The Journal of Physical Chemistry C*, vol. 117, no. 41, pp. 21203-21216, 2013.

[33] A. Soleimani Dorcheh, R. N. Durham, and M. C. Galetz, "Corrosion behavior of stainless and low-chromium steels and IN625 in molten nitrate salts at 600°C," *Solar Energy Materials and Solar Cells*, vol. 144, pp. 109-116, 2016.

[34] P. Vadász, B. Plešingerová, J. Briančin, G. Sučik, and D. Medveď, "Interactions in two-phase systems of MgO(s)-(Na_2O-SiO_2)(l)," *Interceram - International Ceramic Review*, vol. 68, no. 3, pp. 32-39, 2019.

[35] Q. Y. Wang, Y. F. Zhang, S. L. Bai, and Z. D. Liu, "Microstructures, mechanical properties and corrosion resistance of hastelloy C22 coating produced by laser cladding," *Journal of Alloys and Compounds*, vol. 553, pp. 253-258, 2013.

[36] FactSage (8.2). CRCT–ThermFact and GTT–Technologies. Accessed: Jun. 05, 2023. [Online]. Available: https://www.crct.polymtl.ca/ fact/documentation/.